PUBLICATIONS OF THE ASTRONOMICAL SOCIETY OF THE PACIFIC, **116**:797–800, 2004 September

High Spatial Resolution *Hubble Space Telescope* NICMOS Observations of Markarian 231

F. J. LOW, G. SCHNEIDER, AND G. NEUGEBAUER

Steward Observatory, University of Arizona, Tucson, AZ 85721; flow@as.arizona.edu, gschneider@as.arizona.edu, gxn@as.arizona.edu

Received 2004 June 4; accepted 2004 June 15; published 2004 August 23

ABSTRACT. Observations of Markarian 231 at 1.1 μm taken with NICMOS on the *Hubble Space Telescope* are described. The brightness of the object in the near-infrared, and the inherent short-term stability of the NICMOS optical and instrumental system, enables the application of special observational and analysis techniques that effectively increase high spatial resolution. By these means, we set an upper limit on the size of the core of the active galactic nucleus at 8 mas, corresponding to a radial projected distance of ~3 pc from the center of Markarian 231.

1. INTRODUCTION

The ultraluminous infrared galaxy (ULIRG; luminosity $>10^{12}\ L_{\odot}$) Markarian 231 (Mrk 231), which has a bolometric luminosity of $3.3 \times 10^{12}\ L_{\odot}$, was first identified as a ULIRG by Rieke & Low (1972) and was found by the *Infrared Astronomical Satellite* (*IRAS*) survey to be the most luminous object within 300 Mpc (Soifer et al. 1986). The ratio of its flux density at 25 μm (f_{ν}[25]) to its flux density at 60 μm (f_{ν}[60]), $f_{\nu}(25)/f_{\nu}(60) = 0.3$, leads to its inclusion as a "warm" *IRAS* galaxy (Low et al. 1988). It has the visual spectrum of a Seyfert 1 galaxy and a redshift of $z = 0.042$, implying a projected distance scale of 800 pc arcsec^{-1}. From the Two Micron All Sky Survey (2MASS), the near-infrared magnitudes within a 7″ diameter beam of Mrk 231 are J (1.25 μm) = 11.02 mag, H (1.65 μm) = 10.04 mag, and K_S (2.15 μm) = 8.94 mag (Skrutskie et al. 1997). We take the Hubble constant to be $H_0 = 75$ km s^{-1} Mpc^{-1}.

Because Mrk 231 has been considered to be a nearby infrared quasar, several observations over a range of wavelengths have been undertaken to resolve its core. Lai et al. (1998), using adaptive optics with the 3.6 m diameter Canada-France-Hawaii-Telescope, set a limit of 0.″11 (90 pc) on the size of the full width at half-maximum (FWHM) of the core of the active galactic nucleus (AGN) in the near-infrared. Quillen et al. (2001) included Mrk 231 in a survey of unresolved continuum sources at 1.6 μm using the *Hubble Space Telescope* (*HST*); they set a FWHM limit for Mrk 231 of ≤0.″13 (100 pc). Soifer et al. (2000), using the 10 m diameter Keck Telescope, set a limit on the size of the AGN core of 0.″13 (100 pc) at 12.5 μm. Klöckner et al. (2003) report that the hydroxyl megamaser emission shows the characteristics of a rotating, dusty, molecular torus (or thick disk) located between 30 and 100 pc from the central engine of Mrk 231. Lonsdale et al. (2003) showed, from *VLBI* continuum imaging observations, that at 18 cm wavelength, Mrk 231 consists of a single core with FWHM < 0.″005 (4 pc), plus a 0.″03 extension to the south. Further discussion of the galaxy, and references emphasizing other important aspects of the observations of Mrk 231, are given, e.g., in Lonsdale et al. (2003) and Smith et al. (1995).

The capability of using the *HST* at near-infrared wavelengths, plus its short-term (intraorbit) optical stability (Schneider et al. 2001), and the extreme brightness of Mrk 231, offer a singular opportunity to set physically interesting limits on the size of the core in the near-infrared. In this paper, we present observations of Mrk 231 made with NICMOS on the *HST* that were specially designed and optimized to probe the pointlike source in Mrk 231.

On the basis of its far-infrared color, D. C. Hines et al. (2004, in preparation) include Mrk 231 as one of nine hyperluminous and "warm" ULIRGs observed with NICMOS. Although the observations of Mrk 231 in Hines et al. are the same as those shown here, the comparison star used by Hines et al. to define the point-spread function (PSF) differs from the one used here, and their reduction of the image is a preliminary one. The papers by Hines et al. and by Quillen et al. (2001) both include Mrk 231 as one of a larger sample and hence do not attach special attention to the reduction of its data. In this paper, we have concentrated on the reduction of this one object and have attempted to achieve the highest spatial resolution possible with these data.

2. OBSERVATIONS

Observations of Mrk 231 were made in 1998 September using the NIC1 camera and the F110M filter, which has a central wavelength of 1.1 μm and filter FWHM of 0.2 μm, as described by Thompson et al. (1998) and in the NICMOS Instrument Handbook (Roye et al. 2003). The camera has 0.″043 × 0.″043 pixels, corresponding to the diffraction limit of the *HST* at 1.0 μm, and the array has 256 × 256 pixels, so the field of view is ~11″ × 11″. Observations at 1.6 and 2.1 μm using the

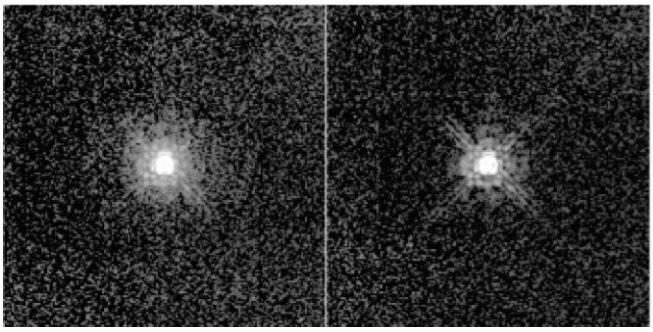

FIG. 1.—NICMOS camera NIC1 F110M images of Mrk 231 (*left*) and PSF reference star GSC 0384500748 (*right*), with the flux density renormalized as discussed in the text. Both images are 7.″5 × 7.″5 and have been constructed from four-point half-integral pixel stepped observations, as described in the text, providing effective spatial sampling of 0.″022 per resampled pixel. Images are shown with a logarithmic stretch of [−2] to [+1] dex ADU s^{-1} $pixel^{-1}$. The diffuse brightening in the circumnuclear region beyond the display-saturated first Airy ring in Mrk 231 compared to GSC 0384500748 is due to the presence of the host galaxy and is to be discussed in G. Schneider & F. J. Low (2005, in preparation).

NIC2 camera accompanied the 1.1 μm observations; these and related observations will be described in G. Schneider & F. J. Low (2005, in preparation).

Four sequential (but separate) images of Mrk 231 were obtained. The observations were made using STEP1/NSAMP = 24 MULTIACCUM sampling (Roye et al. 2003), so the total integration time at the end of the 24 read exposure ramp for each of the individual exposures in the four-point pattern was 22 s. After each exposure, the telescope was offset by a nominal 50.5 pixels, so the active nucleus was centered on different relative positions of a pixel, in addition to sampling different portions of the array. In fact, the observed offsets differed slightly from half-integer pixels, since the pixels projected onto the sky are slightly rectangular, and the average offset was ~50.6 pixels.

Four separate images of the *HST* guide star GSC 0384500748 at right ascension $12^h56^m15\overset{s}{.}8$, decl. +56°48′17.″7 (J2000.0)—a K star—were similarly obtained in the orbit immediately after the Mrk 231 observations, to determine the PSF using the same offset pattern as had been used with Mrk 231. There is no field dependency in the structure of the NIC1 camera PSF star image. The PSF star was selected primarily due to its close proximity (~4′) to Mrk 231 in the sky. The 2MASS survey magnitudes of the PSF star are $J = 11.13$ mag, $H = 10.62$ mag, and $K_S = 10.54$ mag (Skrutskie et al. 1997), so it is of comparable brightness to Mrk 231 in the J band, although fainter at 2.2 μm and considerably less red in its H–K color. Both sets of observations were carried out at the same spacecraft roll angle (i.e., the same field orientation) to minimize changes in differential heating to the optical telescope assembly and to better stabilize the PSF. The time and roll constraints, and the very close proximity of the PSF star in the sky, ensured that the PSF was stable between the Mrk 231 and reference observations.

3. GENERAL RESULTS AND COMMON REDUCTION

The images of Mrk 231 and of the PSF star were first combined to make separate images, each containing a single image of either Mrk 231 or the PSF star, following the precepts outlined in Schneider & Stobie (2002). Image centroids were determined by Gaussian profile fitting after resampling the images onto 32 × finer grids via bicubic interpolation apodized by a sync function. Once the centroids were determined, all images were coaligned by shifting three of the images to the location of the fourth to the nearest integral pixel, and then by interpolative subpixel resampling, also by bicubic sync-apodized interpolation. The four images of the PSF star, which were originally sampled according to the Nyquist criterion with approximately half-pixel offsets, were then median combined after registration, providing supercritical sampling of the PSF star. The final image was resampled onto a grid of 0.″0054 pixels.

The resulting image of Mrk 231 is shown in the left panel of Figure 1. The image of the PSF star is included in the right panel of Figure 1 and is scaled in intensity to "match" the nuclear region of Mrk 231. In the region within a radius of ≤0.″2, the sum of the squares of the subtraction residuals in the difference image was minimized, along with the total energy in the difference image. The imperfectly pupil-plane masked *HST*/NICMOS "diffraction spikes" in the region of radius $r > 0.''2$ were simultaneously minimized. (See Schneider et al. [2001] and Krist et al. [1998] for the details of *HST*/NICMOS target/reference PSF scaling and the effects of mismatched PSF image structures arising from thermal despacing of the *HST* secondary mirror. The effects of temporal variability in pupil mask alignments are also discussed.) Figure 2 shows the median combined azimuthal radial profiles of Mrk 231 and of the PSF star, plus their integrated curves of growth. It is clear that the nuclear region of the 1.1 μm Mrk 231 image is essentially that of an unresolved point source; the FWHM of the raw image of Mrk 231 and of the PSF star is ~0.″10. In Figures 1 and 2, Mrk 231 shows the presence of a host galaxy seen at low surface brightness at a radius greater than 0.″2, but this is better examined by much deeper coronographic imagery and will be discussed in depth by G. Schneider & F. J. Low (2005, in preparation).

3.1. Intrinsic Core Size Limit

To recapitulate, the raw 0.″043 × 0.″043 pixels of NIC1 were oversampled at 1.1 μm through the half-integer pixel offset and the high signal-to-noise ratio available on Mrk 231 to effectively act as 0.″022 × 0.″022 pixels. With such well-sampled images, it was then possible to set a FWHM limit of a putative extension in the nucleus of Mrk 231 that would be well below the classical diffraction limit of the telescope by comparing the

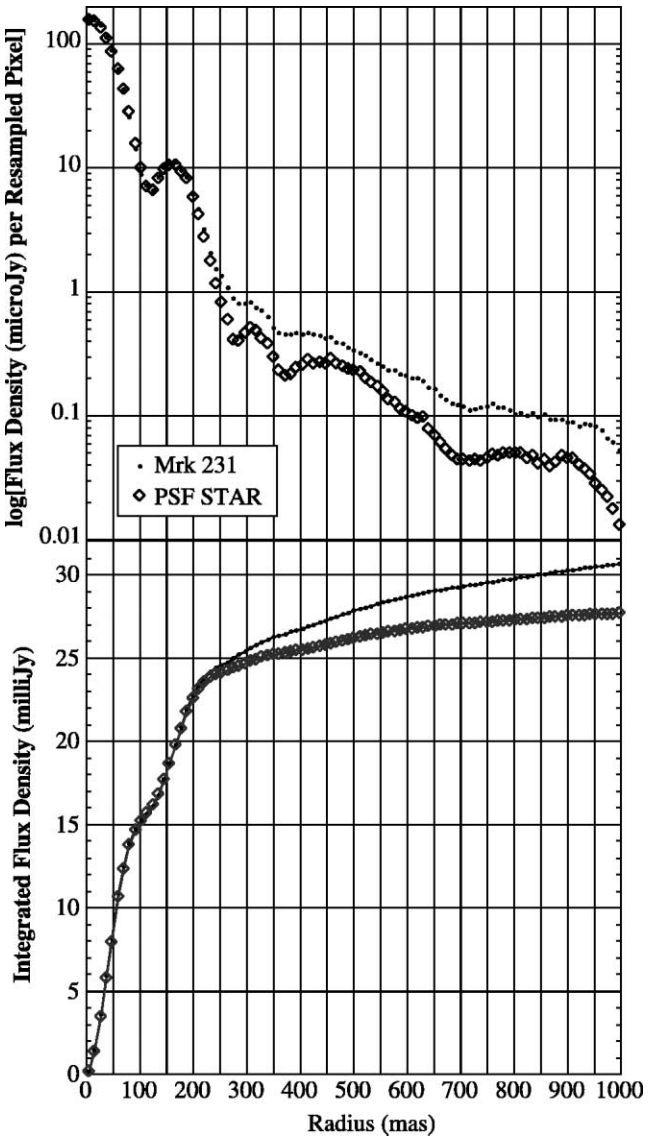

FIG. 2.—Azimuthally median filtered surface brightness radial profiles (*top*) and the integrated flux densities in appropriate annuli (*bottom*) of Mrk 231 and the reference PSF star. The PSF star has been scaled as described in the text and in Schneider et al. (2001) and Krist et al. (1998). It is apparent that the nuclear cores of the two objects are extremely well matched at radii $r < 0\farcs2$. At $r > 0\farcs2$, the contribution to the surface brightness due to the host galaxy is readily apparent (also see Fig. 1).

image structure of the Mrk 231 nucleus to that of a model made up of a core of negligible angular extent plus an assumed extension. We found that radial profiles of PSF-subtracted images using various comparisons were superior in delineating the size of the core as compared to direct techniques (e.g., a Richardson-Lucy deconvolution).

The left panel of Figure 3 shows the result of subtracting the observed image of the PSF star (after registration and flux scaling) from the image of Mrk 231. Images constructed by convolving the observed image of the PSF star with a model

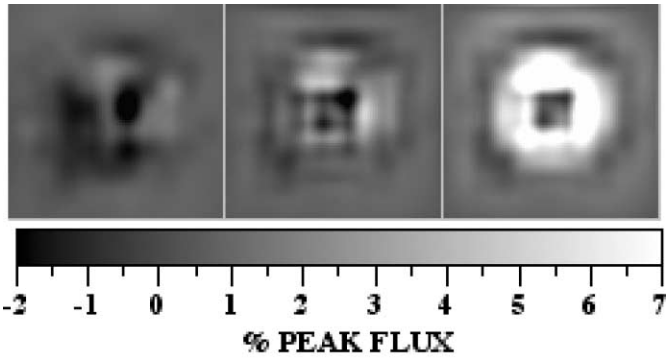

FIG. 3.—Images of Mrk 231 after subtracting the flux-scaled and concentricity-registered reference PSF star image as discussed in text: Mrk 231 as observed (*left*) and as assumed to follow FWHM Gaussian profiles at 5.4 mas (*middle*) and 10.8 mas (*right*). Images extend from −2% (*black*) to +7% (*white*) of the unsubtracted peak intensity of the Mrk 231 nucleus. Images are $0\farcs460 \times 0\farcs460$.

of Mrk 231 in which Mrk 231 is assumed to follow Gaussian profiles of 5.4 and 10.8 mas FWHM are included in Figure 3 (middle and right panels, respectively). We take the similar features seen in the middle and right-hand images of Figure 3 to be a signature of the putative broadening in the Mrk 231 model.

Figure 4 shows the median combined azimuthal radial profiles of the PSF-subtracted images of Figure 3. The three solid curves in the figure refer to putative extensions for the core of Mrk 231, again after subtracting the observed PSF star. The FWHM parameter of the Gaussian profile assumed for Mrk 231 is given in the figure.

In order to test the influence of noise in the image of the PSF star, the image of the observed PSF star was subtracted from a noiseless image of a model NICMOS PSF star[1], as shown by the dotted line in Figure 4. The curves for finite Gaussian extensions are virtually the same, whether the image of the noiseless model PSF or observed PSF stars are subtracted. Additionally, the image of Mrk 231 was itself used in the subtraction, and no significant difference in the final difference image was seen.

The negative residual that arises when normalizing the raw data to the central pixel is not surprising. This zonal undersubtraction is, in fact, replicated using either the observed PSF star (Fig. 4, *dark solid line*) or a noiseless model PSF (*dotted line*), which suggests that this residual is real and is not an artifact of a mismatched PSF. It is consistent with the amount of differential despacing of the *HST* secondary mirror expected between the Mrk 231 and PSF star observations. This residual cannot be explained by extended flux with a Gaussian radial brightness profile, as it would nonphysically imply that the point-source reference PSF star is wider than the core of Mrk 231.

The signature emission seen in Figure 3 is very clearly evident

[1] See http://www.stsci.edu/software/tinytim/tinytim.html.

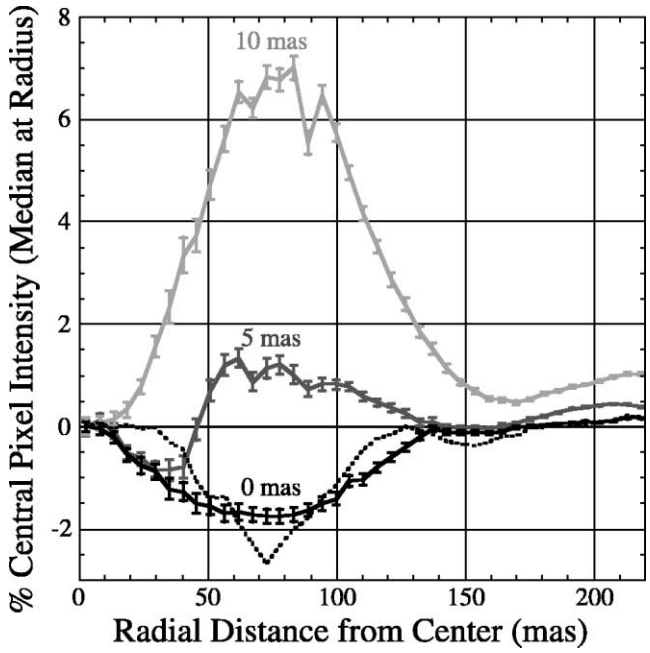

FIG. 4.—Radial brightness profiles (azimuthal median of all pixels in a 5.4 mas wide annuli) of the PSF-subtracted Mrk 231 images shown in Fig. 3. As discussed in the text, the solid lines refer to the FWHM of Gaussian profiles assumed for the core of Mrk 231. The curve marked "0 mas" represents the image of the observed PSF star. The subtraction of a noiseless high-fidelity model PSF (rather than the image of the observed PSF star) from the observed Mrk 231 image is shown by the dotted line. Error bars represent standard deviations (1 σ) of all pixels in each annulus around the median value in each annulus.

in Figure 4 as a nonzero emission peak at a radial distance of ~0.″075—a minimum in the NICMOS diffraction pattern—in the difference image. This can be used to set a limit on the putative extent of the core of Mrk 231. It is clear from Figure 4 that a Gaussian source with a FWHM of 10 mas would be unequivocally detected in the difference image, while a Gaussian profile with a FWHM of 5 mas could be hidden in the data. We will take a FWHM of 8 mas as the limit for the putative extension of Mrk 231.

4. DISCUSSION

4.1. Core Size

In order to place the size limit deduced from these observations into context, it is useful to consider a simple equilibrium thermal model of dust grains surrounding and in thermal equilibrium with a luminous hot central source. At 1.1 μm, the maximum blackbody emission (νf_ν) occurs at a temperature of ~3000 K. Dust grains, however, sublimate at a temperature of ~2000 K, so a temperature of 2000 K for the dust grains is assumed. If the central source has a bolometric luminosity of $3.3 \times 10^{12}\ L_\odot$, blackbody grains 0.17 pc from the central source come to equilibrium at this temperature. Silicate grains about 6× further out, or 1 pc from the central source, come to equilibrium. The size limit we have deduced from these observations and NICMOS is a Gaussian FWHM of 8 mas, or a projected radial distance of 3 pc at 1.1 μm. Although this is significantly smaller than previously published near-infrared limits, this does not restrict physically possible models.

We thank Paul S. Smith and Dean Hines for help with the manuscript and source selection. We also thank an anonymous referee for valuable suggestions. This work was supported in part by NASA grant NAG 5-3042 and 10843 to the NICMOS Instrument Definition and Guaranteed Time Observing teams. This paper is based on observations with the NASA/ESA *Hubble Space Telescope*, operated by the Space Telescope Science Institute, which is operated by the Association of Universities for Research in Astronomy, Inc., under NASA contract NAS 5-26555.

REFERENCES

Klöckner, H.-R., Baan, W. A., & Garrett, M. A. 2003, Nature, 421, 821
Krist, J. E., Golimowski, D. A., Schroeder, D. J., & Henry, T. J. 1998, PASP, 110, 1046
Lai, O., Rouan, D., Rigaut, F., Arsenault, R., & Gendron, E. 1998, A&A, 334, 783
Lonsdale, C. J., Smith, H. E., & Diamond, P. J. 2003, ApJ, 592, 804
Low, F. J., Cutri, R. M., Huchra, J. P., & Kleinmann, S. G. 1988, ApJ, 327, L41
Quillen, A. C., et al. 2001, ApJ, 547, 129
Rieke, G. H., & Low, F. J. 1972, ApJ, 176, L95
Roye, E., et al. 2003, NICMOS Instrument Handbook, Ver. 6.0 (Baltimore: STScI)
Schneider, G., Becklin, E. E., Smith, B. A., Weinberger, A. J., Silverstone, M., & Hines, D. 2001, AJ, 121, 525
Schneider, G., & Stobie, E. 2002, in ASP Conf. Proc. 281, Astronomical Data Analysis Software and Systems XI, ed. D. A. Bohlender, D. Durand, & T. H. Handley (San Francisco: ASP), 382
Skrutskie, M. F., et al. 1997, in The Impact of Large Scale Near-IR Sky Surveys, ed. F. Garzon et al. (Dordrecht: Kluwer), 25
Smith, P. S., Schmidt, G. D., Allen, R. G., & Angel, J. R. P. 1995, ApJ, 444, 146
Soifer, B. T., et al. 2000, AJ, 119, 509
———. 1986, ApJ, 303, L41
Thompson, R., Rieke, M., Schneider, G., Hines, D., & Corbin, M. 1998, ApJ, 492, L95